International Journal of Sustainability in Research (IJSR)
Vol. 4, No. 3, 2026 : 115-134

Improved Graphene-Based Sodium-Ion Battery Anodes Using Low Surface Area and Tempreture

Uqab Afridi[1*]
College of Materials Science and Engineering, Hohai University
Corresponding Author: Uqab Afridi uqabafridi9@gmail.com

A R T I C L E I N F O

Keywords: Sodium-Ion Battery, Graphene, Temperature, Low Surface Area

Received : 21, March
Revised : 23, April
Accepted: 25, May

A B S T R A C T

Reduced graphene oxide (rGO) has emerged as a strong candidate for high-capacity anodes in sodium-ion batteries, yet its inherently large specific surface area—mainly caused by structural exfoliation during reduction promotes excessive solid–electrolyte interphase (SEI) growth, resulting in substantial irreversible capacity during early cycles. To address this drawback, we developed a strategy to produce rGO powders with controlled, low surface area by combining spray drying with gradual thermal reduction, thereby suppressing over-exfoliation. Electrodes fabricated from these powders and reduced at different temperatures (200–1000 °C) were systematically compared with high-surface-area counterparts to disentangle the contributions of oxygen functionality and surface area to electrochemical behavior. The optimized sample reduced at 400 °C delivered the most favorable performance, achieving a reversible capacity of 216 m Ah g^{-1} at 100 mA g^{-1} and maintaining 85% of its capacity after 200 charge–discharge cycles. Furthermore, irreversible capacity loss was diminished by a factor of two to three relative to earlier reports. Although further refinement is needed to achieve full commercial viability, these findings underscore the importance of morphological control strategies that minimize surface area, promote structural restacking, and optimize oxygen functional group content to enhance the long-term performance of rGO-based sodium-ion battery anodes.

DOI: https://doi.org/10.59890/ijsr.v4i3.400
ISSN-E: 3025-7379
https://dmimultitechpublisher.my.id/index.php/ijsr

INTRODUCTION

Sodium-ion batteries (SIBs) have emerged as a competitive alternative to lithium-ion batteries (LIBs) due to the natural abundance and low cost of sodium compared to lithium [1]. Although both systems operate on similar electrochemical principles, the larger ionic radius of Na^+ (1.02 Å) relative to Li^+ (0.76 Å) results in sluggish diffusion kinetics and more challenging intercalation, which significantly restrict the overall electrochemical performance of SIBs [2].

Graphite, which serves as the dominant anode in LIBs, is unsuitable for SIBs because Na^+ intercalation requires much higher energy (1.51 eV/Na^+ compared with 0.53 eV/Li^+). Furthermore, the intrinsic interlayer spacing of graphite (0.335 nm) is insufficient for Na^+ insertion, as at least 0.37 nm is necessary for stable accommodation within carbon lattices [3]. These inherent constraints have motivated extensive research into carbon-based materials with enlarged interlayer spacing and engineered architectures that can facilitate sodium storage. Among these alternatives, hard carbon has been widely recognized as a leading anode material due to its relatively low production cost, large interlayer gaps, and good cycling stability [4, 5]. Nevertheless, hard carbon is limited by its modest initial coulombic efficiency (ICE, typically ~80%) and sluggish electrochemical kinetics, which hinder its rate capability [6]. In addition, the underlying Na^+ storage mechanism in hard carbon is still not fully understood, making it difficult to optimize material design [4,6]. Strategies such as presodiation and the use of biomass-derived carbons have been investigated to enhance electrochemical performance [7, 8]. Although these methods improve ICE, the dominant storage process—Na^+ insertion into closed pores—remains diffusion-limited, reducing the high-rate performance of the electrode [9]. These limitations have encouraged exploration of alternative amorphous carbon materials that can provide higher capacity with faster reaction dynamics. Reduced graphene oxide (rGO) has gained considerable interest for application in both LIBs and SIBs, owing to its tunable structural features, high theoretical capacity, and versatile synthesis routes. Typically, rGO is derived from graphene oxide (GO), which is rich in oxygen-containing groups—often exceeding 50 wt% when prepared by the Hummers' method. While these functional groups impair the electrical conductivity of GO, rendering it unsuitable as an electrode [10, 11], different reduction techniques have been developed to restore conductivity. These include chemical [12], thermal [13], electrochemical [14], and microwave-assisted reduction methods [15] all of which yield few-layer graphene-like nanosheets. The resulting rGO generally exhibits a high specific surface area (SSA), providing numerous electrochemically active sites for both Li^+ [16, 17] and Na^+ storage [18, 19]. However, the large SSA also promotes extensive side reactions, leading to low ICE values (often <60%). Despite this, rGO demonstrates outstanding reversible capacity, with some reports achieving values as high as 603 m Ah g^{-1} at 0.05 A g^{-1}[18, 20].

The first use of thermally exfoliated reduced graphene oxide (rGO) as an anode in sodium-ion batteries (SIBs) was demonstrated by Wang et al., who

reported a low initial coulombic efficiency (ICE) of 18% and a reversible capacity of 173 m Ah g^{-1} at 0.04 A g^{-1} [20]. Since that report, extensive efforts have been devoted to studying rGO, both as a standalone anode and as a component in composites, with many studies showing notable improvements in rate capability [18, 21, 22]. Despite these advances, most rGO materials possess extremely high specific surface areas (SSA, typically 500–1000 m^2 g^{-1}). Although a large SSA provides abundant active sites for sodium storage, it simultaneously accelerates side reactions with the electrolyte and increases solid electrolyte interphase (SEI) formation, leading to substantial irreversible capacity loss and reduced cycling stability [23]. Therefore, the central challenge for rGO-based anodes is to balance capacity and reversibility by optimizing SSA to limit parasitic reactions while still maintaining sufficient storage sites for Na^+.

The reduction–exfoliation process is a key factor governing the SSA of rGO since it directly influences particle aggregation and porosity [24, 25]. During thermal reduction, graphene oxide (GO) undergoes rapid self-heating reactions that release gases such as CO, CO_2, and H_2O. The sudden evolution of these gases causes violent exfoliation of GO layers, producing porous, airy rGO structures with high surface area [13]. Controlling the heating profile is therefore critical. If sufficient time is allowed for gas diffusion, pressure buildup can be reduced, preventing explosive exfoliation. For example, McAllister et al. showed that using a slow heating rate (<1 °C min^{-1}) effectively suppresses violent exfoliation [24]. Thus, the heating rate can be used as a tuning parameter to produce either low-SSA or high-SSA rGO materials [26]. Even with optimized thermal treatment, rGO often retains oxygen-containing functional groups and structural defects. These residual sites can serve as strong binding centers for sodium ions, hindering desodiation and lowering reversibility [27-29]. Furthermore, because both SSA and chemical functionalities evolve during reduction, their effects on electrochemical behavior are often intertwined. Misattribution of capacity contributions to either surface area or chemical bonding complicates interpretation. As a result, systematically decoupling the influence of SSA from chemical defects is essential for developing a clear understanding of the structure–property relationships in rGO-based anodes.

The aim of this work is to disentangle the respective roles of reduced graphene oxide surface chemistry and electrolyte-accessible specific surface area in governing sodium-ion storage properties such as insertion behavior, cycling stability, and irreversible capacity loss. For this purpose, we compared sodium anodes fabricated from exfoliated rGO powders with those prepared from powders reduced to a similar chemical state but intentionally kept unexfoliated. To achieve low SSA, GO precursors were first processed by spray-drying ethanol-based suspensions, which induced granulation and stacking of the sheets. This compact structure was preserved during reduction, preventing exfoliation, lowering SSA, and ultimately enhancing the initial coulombic efficiency.

Systematic heat-treatment experiments were conducted between 200 and 1000 °C, with 400 °C selected as the baseline reduction temperature. The

significance of this structural control is evidenced by our optimized non-exfoliated rGO anodes, which deliver a robust reversible capacity of 216 mAh g^{-1} at 100 mA g^{-1} and maintain 85% capacity retention after 200 cycles. Most notably, this approach diminishes the irreversible capacity loss by a factor of two to three compared to earlier reports for rGO anodes. Furthermore, our findings demonstrate a crucial manufacturing advantage: unlike exfoliated materials that yield highly viscous slurries requiring excessive solvent, the non-exfoliated powders enable the fabrication of slurries with significantly higher solid loading. These observations not only resolve the fundamental debate regarding the dominant factors in overall cell efficiency—proving that SSA has a more decisive impact than structural chemistry alone—but also provide a scalable, practical pathway for the commercial development of high-performance rGO-based SIBs.

LITERATURE REVIEW

This article discusses the development of reduced graphene oxide (rGO)-based anode materials for sodium-ion batteries (SIBs), which are considered a promising alternative to lithium-ion batteries due to the abundance and lower cost of sodium resources. The authors highlight that although rGO offers high capacity, its large specific surface area—resulting from the reduction process—often leads to excessive formation of the solid–electrolyte interphase (SEI). This phenomenon contributes to significant irreversible capacity loss during the initial cycles, which remains a major challenge in utilizing rGO as an anode material.

Previous studies have explored various strategies to enhance the performance of rGO, including structural modification, heteroatom doping, and morphology control. However, many of these approaches still face a trade-off between achieving high surface area (which improves electrochemical activity) and maintaining cycling stability, as higher surface area tends to accelerate SEI formation. This article reinforces earlier findings that controlling microstructure—particularly surface area—is a critical factor in improving the electrochemical efficiency of graphene-based materials.

The study introduces a novel approach by combining spray drying with stepwise thermal reduction to produce rGO with a lower specific surface area. This method aims to prevent over-exfoliation, which commonly occurs during conventional reduction processes. By comparing samples reduced at different temperatures (ranging from 200 to 1000 °C), the authors systematically investigate the effects of surface area and oxygen-containing functional groups on battery performance, offering valuable insights into the underlying material behavior.

The results indicate that the sample reduced at 400 °C delivers the best performance, achieving a reversible capacity of 216 mAh g^{-1} at a current density of 100 mA g^{-1} and maintaining 85% capacity retention after 200 cycles. Furthermore, the irreversible capacity loss is reduced by two to three times compared to previously reported studies. These findings suggest that an optimal balance between low surface area and an appropriate amount of

oxygen functional groups is essential for enhancing both the stability and efficiency of rGO anodes.

Overall, this article emphasizes the importance of morphological engineering in the development of anode materials for sodium-ion batteries. By reducing surface area and carefully tuning the internal structure of rGO, long-term electrochemical performance can be significantly improved. Although further research is needed to achieve commercial viability, this study provides an important contribution toward the design of more efficient and sustainable energy storage materials.

METHODOLOGY

Synthesis of rGO materials

Graphene oxide was produced using a modified Hummers' method with graphite particles as the raw material (Alfa Aesar, 10 mesh, 99% purity) [10, 28]. In a typical synthesis, a 9:1 volume ratio of sulfuric acid (H_2SO_4, Sigma-Aldrich) and phosphoric acid (H_3PO_4, 95 wt%, Sigma-Aldrich) was transferred into an 800 mL reaction flask. Under continuous stirring, 6 g of graphite and 36 g of potassium permanganate ($KMnO_4$, ACS grade, LabChem) were gradually added. The suspension was kept at 52 °C for 17 h to allow oxidation. After the reaction, the mixture was cooled and poured onto 800 g of ice, followed by slow addition of ~20 mL of hydrogen peroxide solution (H_2O_2, 30 wt% in water, Sigma-Aldrich), which changed the mixture color from purple to yellow, confirming the oxidation process. The crude product was purified through multiple centrifugations and washing steps. The slurry was first washed twice with 20 wt% hydrochloric acid (HCl, Sigma-Aldrich) to remove metal ions, followed by four rinses with ethanol. The purified GO was re-dispersed in ethanol to prepare a 12 g L^{-1} suspension. This dispersion was stirred for 6 h and then subjected to sonication (Sonics Vibra Cell, 60% amplitude, 10 min) to ensure uniform exfoliation. The well-dispersed suspension was dried using a BUCHI B-290 Mini Spray Dryer under the following operating conditions: nitrogen flow of 601 L h^{-1}, pump power set to 30%, aspirator at 100%, inlet temperature of 180 °C, and feed solution concentration of 12 g L^{-1}. To maintain oxygen-free conditions and recover ethanol safely, a BUCHI Inert Loop B-295 unit was employed, minimizing explosion risk. The spray-dried GO powders were reduced in a tube furnace (Thermo Scientific, Lindberg Blue M) under a 95% Ar / 5% H_2 reducing atmosphere. The reduction parameters, including heating rate and maximum temperature, were adjusted to tailor the specific surface area (SSA). Faster heating promoted exfoliation and generated high-SSA rGO, while slower heating suppressed exfoliation, yielding low-SSA rGO. Approximately 200 mg of GO powder was placed in an alumina crucible (MTI Corporation) for each heating cycle. Reduction was carried out at maximum temperatures of 200, 300, 400, 600, 800, and 1000 °C. The reduced graphene oxide (rGO) powders were collected after cooling and used directly without further modification.

Preparation of electrodes ppm

For the preparation of electrodes from non-exfoliated rGO, a water-based slurry was formulated containing rGO powder (active material), sodium alginate binder (Acros Organics), and Super C45 conductive carbon (MTI Corporation) in a mass ratio of 70:20:10. The resulting slurry contained ~8 wt% solids. For comparison, unreduced GO electrodes were made from a separate slurry composed of GO, Super C45, and sodium alginate in a 50:30:20 weight ratio. Owing to the higher oxygen content of GO, the maximum solid loading was restricted to ~6 wt%. Both slurries were coated onto copper foil (15 µm thick) using a doctor blade (MTI Corporation) with a wet film thickness of 50 µm, and the coatings were dried overnight at 110 °C. Circular electrodes (12.7 mm in diameter) were then punched and transferred into an argon-filled glovebox (Inert IL-2BG, <1 ppm O_2 and H_2O) for coin-cell assembly.

Electrodes based on high-surface-area (high-SSA) rGO required a different approach, as the powders could not be processed into stable, concentrated slurries. In this case, exfoliated rGO powders were directly embedded into copper mesh discs (12.7 mm diameter, McMaster-Carr). The powders were compacted using a die press (MTI Corporation) at ~69 MPa for 2 minutes, ensuring firm adhesion to the mesh.

CR2032-type coin cells (MTI Corporation) were assembled inside the glovebox using the prepared working electrodes, sodium metal foil (Sigma-Aldrich) as the counter/reference electrode, and glass fiber filters (Whatman, 1.6 µm pore size) as separators. The electrolyte was 1 M Na PF_6 dissolved in a 1:1 (v/v) mixture of ethylene carbonate (EC) and dimethyl carbonate (DMC).

Material characterization

The crystalline structure of the prepared materials was examined by X-ray diffraction (Rigaku Miniflex II) within a 2θ range of 5°–40°, applying a scan rate of 1° min^{-1}. The specific surface area of the samples was quantified using nitrogen adsorption at 77.3 K, based on the Brunauer–Emmett–Teller (BET) method, with measurements carried out on a Micromeritics Gemini 2390a analyzer. X-ray photoelectron spectroscopy (XPS; Thermo Scientific K-Alpha) was performed to investigate the surface chemistry of GO, rGO, and exfoliated rGO (rGOexf). The measurements were conducted at room temperature using Al Kα radiation (1486.6 eV) as the excitation source. All samples were handled inside an argon-filled glovebox and transferred to the XPS chamber via an argon-sealed transfer vessel (Thermo Scientific 831-57100-2) to minimize air exposure. The resulting spectra were processed using Casa XPS software, with binding energies referenced to the C1s signal of adventitious carbon (284.8 eV).

Electrochemical measurements

The electrochemical characterization of the assembled cells was performed using a LAND battery testing system (LAHNE). To determine rate capability, the cells were subjected to sequential cycling at current densities of 100, 200, 500, 1000, 2000, and 4000 mA g^{-1}. Each step consisted of four cycles, following an initial formation cycle at 100 mA g^{-1}. The current density was then reduced back to 100 mA g^{-1} for an additional four cycles to evaluate recovery. Cyclic voltammetry (CV) was conducted on a Bio-Logic SP-200 workstation over the potential range of 0.05–2.0 V, with a scan rate of 0.5 mV s^{-1}. For long-

term cycling performance, the cells underwent 15 preliminary cycles at 100 mA g^{-1}, followed by continuous cycling for 200 cycles at 1000 mA g^{-1}. Unless otherwise stated, all electrochemical tests were carried out within a voltage window of 0–2.0 V.

RESEARCH RESULT AND DISCUSSION

Material characterization

The central aim of this study was to prepare graphene oxide (GO) powders with intrinsically low specific surface area (SSA) and to examine whether this compact morphology could be preserved after controlled thermal reduction. A GO dispersion, derived from the final washing step of the modified Hummers' method, was spray-dried in ethanol at a feed concentration of 12 g L^{-1}. Ethanol-assisted spray drying enables the use of more concentrated dispersions compared to water-based systems, which favors particle agglomeration and thus lowers SSA. This process yielded GO powders (Figs. 1a, b) with an SSA of 25.3 m^2 g^{-1}. Following thermal reduction, the non-exfoliated samples retained similarly low surface areas (15–40 m^2 g^{-1}), close to that of the precursor GO. In contrast, exfoliated samples showed a dramatic increase in SSA, reaching 200–600 m^2 g^{-1} (Fig. 1b).

The reduced GO samples were identified by both treatment temperature and exfoliation history, i.e., rGO200, rGO200exf, rGO300, rGO300exf, rGO400, rGO400exf, rGO600, rGO600exf, rGO800, rGO800exf, rGO1000, and rGO1000exf. Slow heating of GO, high-SSA rGOexf, and low-SSA rGO at 0.5 °C min^{-1} in the 150–300 °C range led to extensive decomposition of GO into rGO [24]. BET analysis confirmed these SSA differences, with exfoliated samples exhibiting much higher values than their compact, non-exfoliated counterparts. The visual comparison was also striking: GO, rGO400, and rGO400exf, although equal in mass, occupied very different volumes (Fig. 1c). The rGO400exf appeared light and fluffy, nearly filling its container, whereas GO and rGO400 were denser, sand-like, and settled compactly at the bottom.

These findings highlight the critical role of exfoliation during reduction in shaping the final morphology and SSA of rGO. The heating rate was found to be decisive: when heated rapidly (≥ 5 °C min^{-1}), oxygen functionalities decomposed abruptly, generating CO, CO_2, and H_2O gases. The rapid gas release caused internal pressure buildup and violent sheet expansion, giving rise to porous rGO with high SSA. In contrast, when heating proceeded slowly (≤ 1 °C min^{-1}), the gases escaped gradually, avoiding pressure accumulation and thereby preserving the layered arrangement of GO. This produced dense rGO with limited SSA and fewer reactive sites for side reactions with the electrolyte. By tuning the heating rate, it is therefore possible to regulate the SSA of rGO while retaining similar oxygen contents, enabling the independent study of how surface area and chemical composition affect the electrochemical behavior of rGO-based anodes.

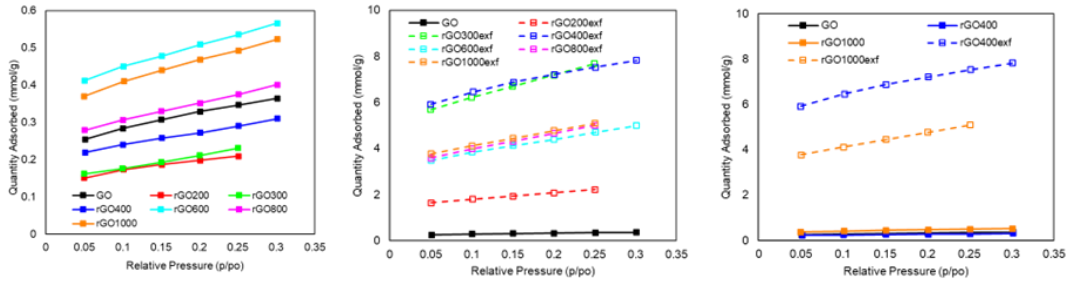

(a) (b) (c)

Figure 1. BET Isotherms for GO, Low SSA rGO, and high SSA rGO powders.

Define XPS characterization provided further clarification of the contrasts between exfoliated and non-exfoliated materials across the entire reduction temperature spectrum (Fig. 2). It was found that exfoliated rGO consistently exhibited higher levels of surface-bound oxygen than non-exfoliated rGO, with the largest discrepancies occurring in the mid-temperature region (400–800 °C). The subsequent discussion focuses on how these chemical differences, combined with surface area effects, impact electrochemical response—particularly in relation to solid–electrolyte interphase (SEI) development and the long-term stability of capacity.

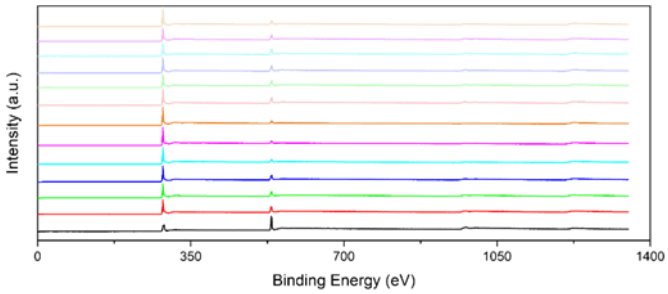

Figure 2. XPS survey spectra for GO, Low SSA rGO, and high SSA rGO powders.

Number XRD measurements demonstrated that both exfoliation and residual oxygen functionalities play key roles in determining the crystallinity and interlayer separation of the samples. As illustrated in Fig. 3, GO exhibits a sharp 001 reflection near $2\theta \approx 9°$, corresponding to an interlayer spacing of about 0.96 nm based on Bragg's law. This expanded spacing, relative to graphite, arises from the incorporation of oxygen-containing groups between the carbon sheets. Following thermal reduction, the non-exfoliated rGO samples show a broad reflection that shifts to $2\theta \approx 23–26°$, signifying a contraction in interlayer distance as oxygen moieties are removed and the carbon network becomes more compact [31]. By contrast, exfoliated rGO displays an absence of well-defined diffraction peaks, consistent with its disordered, amorphous structure, as exemplified by the rGO400exf sample in Fig. 3. With increasing reduction temperature, the interlayer distance in non-exfoliated rGO continues to contract, eventually approaching the spacing of crystalline graphite (0.335 nm) [3].

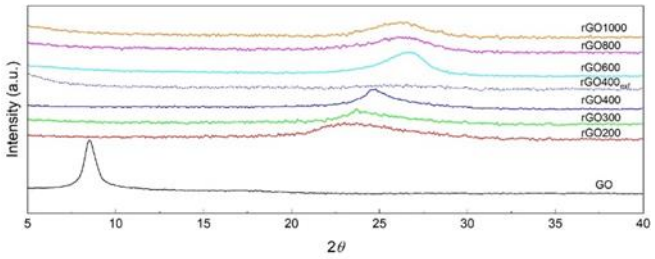

Figure 3. XRD spectra of all samples.

Electrochemical characterization

The electrochemical response of GO, rGO400, rGO1000, and their exfoliated variants was examined by cyclic voltammetry (CV) to probe the role of surface chemistry in capacitive behavior (Fig. 4). During the initial scan of GO, a strong cathodic feature appears below 1.0 V vs. Na/Na^+, which can be attributed to electrolyte breakdown and the irreversible elimination of oxygenated groups. With increasing reduction temperature, this peak gradually weakens, and the CV traces evolve toward a more rectangular shape, consistent with a shift toward double-layer capacitive behavior as oxygen functionality decreases. This trend is especially noticeable for exfoliated materials, which generate higher current densities and larger enclosed areas, reflecting their expanded surface area and abundance of exposed edge sites.

At the same time, exfoliated rGO shows stronger irreversible signals in the first cycle, implying less uniform solid–electrolyte interphase (SEI) formation. The highly porous and reactive structure of these samples likely results in uneven surface coverage or unstable SEI. This interpretation is supported by later cycles, where exfoliated rGO400exf and rGO1000exf display pronounced hysteresis and greater current fading, indicative of inhomogeneous or evolving SEI layers. Although stabilization occurs over extended cycling, the early instability suggests persistent side reactions. In contrast, non-exfoliated samples present smoother and more reproducible CV curves, pointing to the development of more compact and stable SEI coatings.

The rate capability of exfoliated rGO samples (Fig. 5) follows similar trends to their non-exfoliated counterparts, with the notable exception of the 1000 °C case. Among all materials, rGO400, rGO200exf, rGO300exf, and rGO1000exf demonstrate the strongest overall performance. Interestingly, while non-exfoliated rGO1000 shows the weakest response, the exfoliated version (rGO1000exf) delivers enhanced rate behavior compared with samples reduced at other temperatures. This improvement is attributed to the large surface area introduced during exfoliation, which compensates for the narrow interlayer spacing and low oxygen content typical of rGO reduced at 1000 °C. Representative rate tests for the 400 °C and 1000 °C samples are displayed in Figs. 5a and b, with additional comparisons at intermediate reduction temperatures provided in Fig. 5.

At lower reduction temperatures (200–400 °C), the difference between exfoliated and non-exfoliated materials is minor, indicating that increased surface area has little to no negative influence on rate response under these

conditions. This can be explained by the fact that non-exfoliated samples at these temperatures still retain sufficient oxygen functionalities to maintain expanded interlayer spacing, enabling sodium ions to reach internal storage sites in a manner comparable to exfoliated structures. At intermediate reduction levels (600–800 °C), however, the non-exfoliated samples outperform the exfoliated ones. Although these materials possess narrower interlayer distances and fewer oxygen groups, the excessive surface area of exfoliated samples at these temperatures likely accelerates solid–electrolyte interphase (SEI) growth, consuming active sites and restricting Na^+ diffusion, thereby suppressing their capacity.

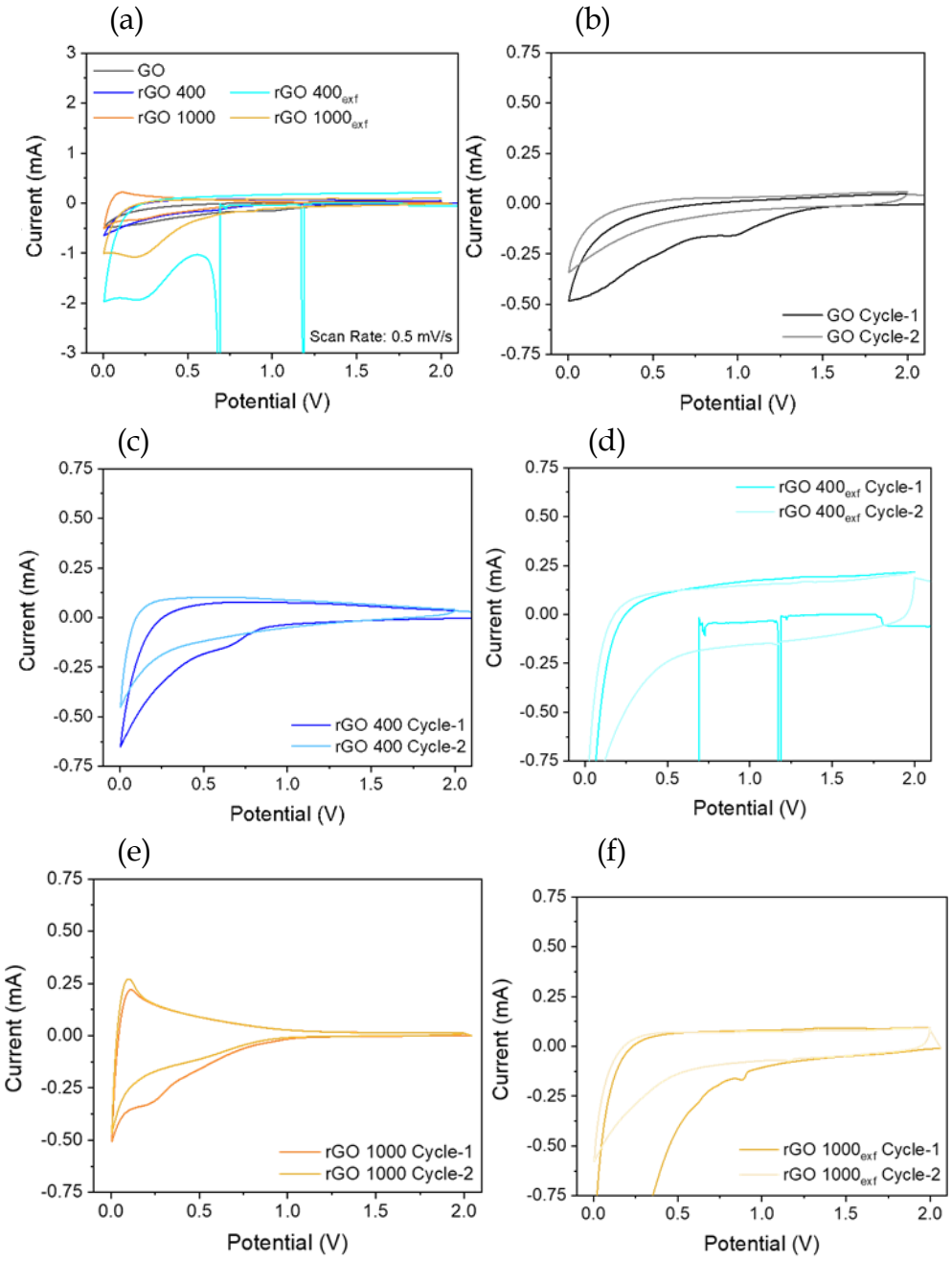

Figure 4. CV curves (a) 1st cycles of GO, rGO400, rGO1000, rGO400exf, and rGO1000exf. (b-f) 1st and 2nd cycles comparison of (b) GO, (c) rGO400, (d) rGO1000, (e) rGO400exf, and (f) rGO1000exf.

A contrasting trend is observed at 1000 °C, where exfoliation clearly enhances performance. In this case, the limited oxygen functionality and tightly packed layers in non-exfoliated rGO1000 severely constrain Na^+ storage. Exfoliation mitigates this issue by introducing a large accessible surface, which provides sufficient adsorption sites to offset the structural limitations. As a result, rGO1000exf is the only sample where exfoliation delivers a marked advantage over the non-exfoliated form.

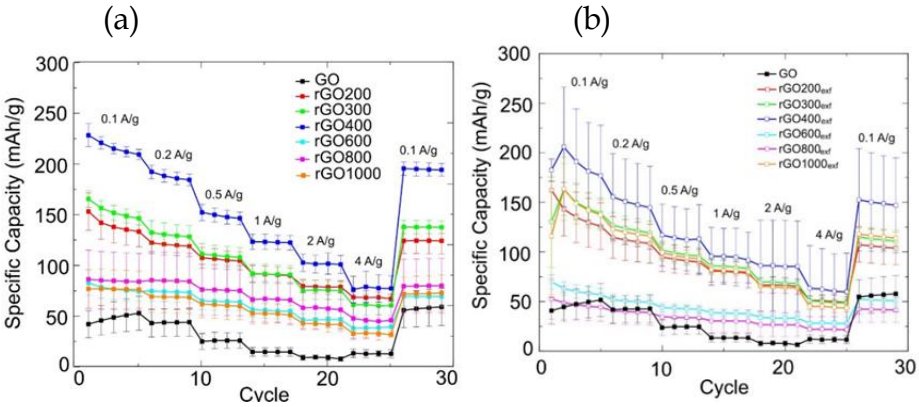

Figure 5. Mean rate capability performance of (a) non-exfoliated materials and (b) exfoliated materials. Errors bars indicate the corresponding standard deviation from three cells. All measurements were conducted at an active material mass loading of 0.8 mg cm-2.

The Coulombic efficiency profiles of all electrodes are presented in Fig. 6. For non-exfoliated samples, the initial Coulombic efficiencies range between 45–60%, aligning with reported values for carbon-based anodes in sodium-ion batteries [33, 34, 35]. Despite this agreement, such levels are still below the threshold required for practical applications. Within this group, rGO400 shows the most favorable behavior, achieving the highest two-cycle CE and displaying clear improvement after the first cycle. In contrast, exfoliated electrodes exhibit considerably lower ICEs, with the best case reaching only about 20%. This poor performance can be attributed to extensive solid electrolyte interphase (SEI) growth during the initial cycles, driven by their significantly larger electrochemically active surface area, which results in substantial irreversible Na^+ loss. By comparison, the denser structure of non-exfoliated samples restricts SEI formation and limits sodium consumption, underlining a major benefit of their more compact morphology.

As illustrated in Fig. 6, exfoliated electrodes (open symbols) typically require about ten cycles before reaching Coulombic efficiencies comparable to non-exfoliated samples (closed symbols). Furthermore, while the CE of non-exfoliated materials approaches 100% during the final four cycles—when the current density is stepped back to 100 mA g^{-1} exfoliated electrodes exhibit a secondary efficiency drop. This indicates that un passivated regions in exfoliated structures become electrochemically active only at lower current densities, where Na^+ ions can infiltrate deeper or into more tortuous pores, initiating further SEI growth and additional sodium consumption. Conversely,

the more compact architecture of non-exfoliated materials promotes uniform SEI formation during the early cycles, thereby preventing this secondary decline.

During long-term cycling, rGO400 maintains the most stable and reliable performance across both reduction temperatures and exfoliation conditions. Nevertheless, the gap between exfoliated and non-exfoliated electrodes is narrower here than in rate performance tests. Notably, all thermally reduced rGO electrodes substantially outperform unreduced graphene oxide, which shows capacities below 10 m Ah g^{-1} at 1 A g^{-1}. This demonstrates that unreduced GO, due to its excessive oxygen functional groups and large interlayer spacing, is intrinsically unsuitable as a sodium-ion battery anode.

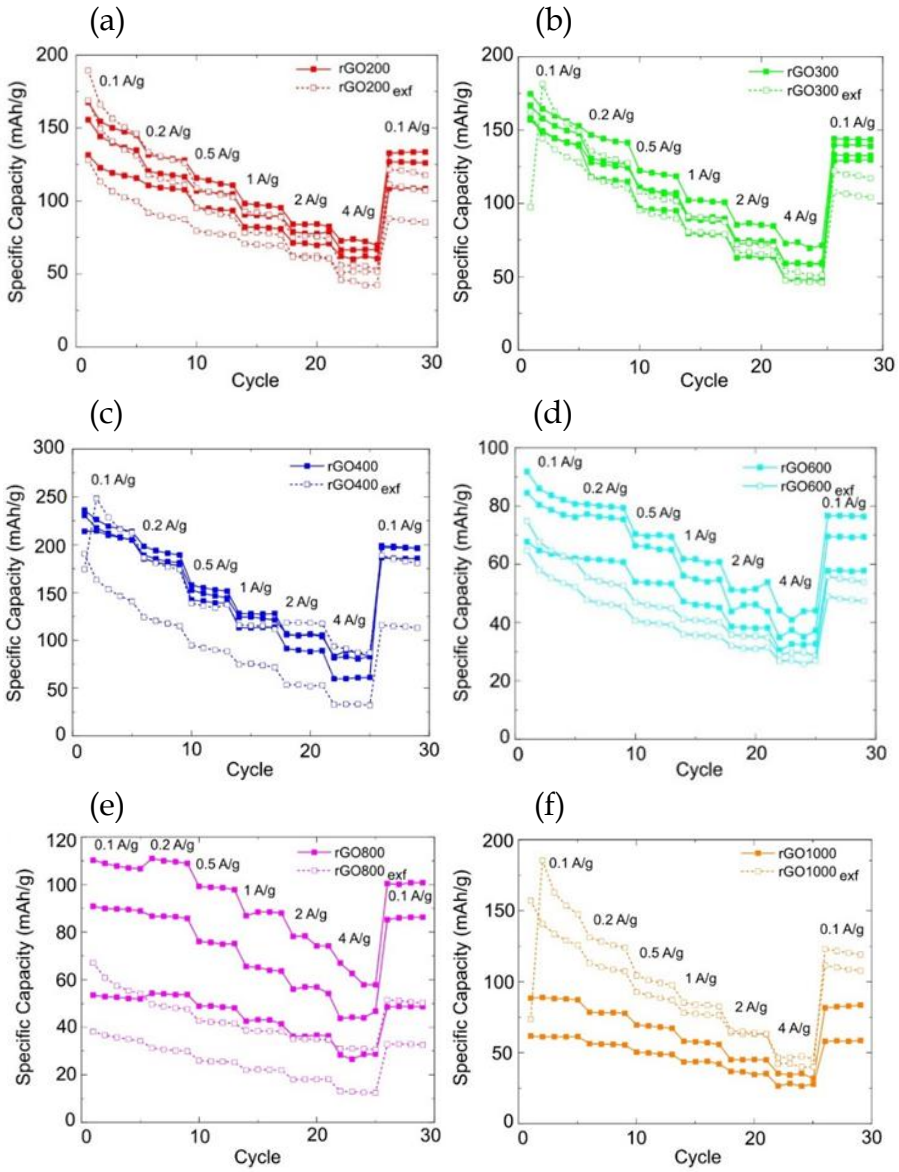

Figure 6. Rate capability comparison for (a) rGO200 versus rGO200exf, (b) rGO300 versus rGO300exf, (c) rGO400 versus rGO400exf, (d) rGO600 versus rGO600exf, (e) rGO800 versus rGO800exf, and (f) rGO1000 versus rGO1000exf. The active material loading used is 0.8 mg cm-2.

The cycling stability of electrodes prepared from non-exfoliated materials is strongly dependent on the reduction temperature. As illustrated in Fig. 6a, electrodes reduced at lower temperatures (200 °C, 300 °C, and 400 °C) retain capacity more effectively than those treated at higher temperatures (600 °C, 800 °C, and 1000 °C). Here, 100% retention refers to the capacity measured in the 16th cycle—the first cycle at 1 A g^{-1} following 15 conditioning cycles at 100 mA g^{-1}. Electrodes processed at higher temperatures suffer from a steep initial capacity drop those later levels off, whereas those reduced at lower temperatures show a slower, more progressive decline within the first 25 cycles. The rapid fading in high-temperature samples can be linked to irreversible sodium trapping between tightly stacked graphene sheets in highly graphitized structures, which reduces the number of accessible storage sites.

After 200 cycles (Fig. 6b), all electrodes retain less than 80% of their initial capacity. Among exfoliated samples, rGO400exf exhibits the weakest retention, while rGO1000exf achieves the best. Unlike the non-exfoliated group, exfoliated electrodes show no consistent trend between reduction temperature and long-term stability. Their poorer cycling behavior is likely related to the fragile SEI formed on their high-surface-area structures; repeated cracking and reformation consume sodium irreversibly and compromise cycle life. The retention and long-term cycling behavior for selected samples treated at 400 °C and 1000 °C are compared in Fig. 6c and d.

Over extended operation, non-exfoliated electrodes consistently deliver higher specific capacities and better capacity retention than their exfoliated counterparts, though this advantage diminishes at higher reduction temperatures. Their denser structure and controlled surface exposure limit SEI overgrowth and mitigate mechanical deterioration, enabling more stable cycling performance. These features underline their potential suitability for sodium-ion battery anodes.

To gain further insight into the storage mechanism, sodiation/desodiation voltage profiles of the best-performing samples—rGO400 (non-exfoliated) and rGO400exf (exfoliated)—were examined (Fig. 7). At a current density of 0.1 A g^{-1}, the second cycle reveals distinct differences at low voltages. The rGO400exf electrode displays an extended low-voltage plateau, characteristic of ongoing SEI growth. In comparison, rGO400 shows such a plateau only in the first two cycles, after which it disappears, suggesting that non-exfoliated electrodes establish a stable SEI more quickly than exfoliated ones.

A noticeable voltage shift at comparable capacities indicates that the exfoliated electrode experiences considerable overpotentials during both sodiation and desodiation. Nonetheless, the overall shapes of the desodiation profiles for rGO400 and rGO400exf at different current densities remain similar, suggesting that both materials rely on comparable sodium storage mechanisms. The rightward displacement of the rGO400exf curve during sodiation is likely associated with greater irreversible capacity loss, while the leftward shift after desodiation can be attributed to a larger internal resistance drop resulting from a thicker SEI layer. These findings correspond well with the Coulombic

efficiency data, showing that the higher surface area of exfoliated rGO promotes accelerated electrolyte decomposition and delays SEI stabilization. Similar effects have been documented in lithium–silicon electrodes, where the growth of thick SEI films on high-surface-area materials hinders ionic transport and slows charge kinetics. In sodium-ion systems, these challenges are likely amplified because of the larger ionic radius and slower diffusion of Na^+. To substantiate this interpretation, further work is needed to characterize the SEI's structure, composition, and ion transport properties in exfoliated and non-exfoliated rGO electrodes using advanced tools such as electrochemical impedance spectroscopy (EIS), cryo-TEM, and time-of-flight secondary ion mass spectrometry (TOF-SIMS). Such analyses will be critical for optimizing SEI properties and enhancing the cycling stability of practical Na-ion battery anodes.

Comparison of electrochemical results confirms that non-exfoliated materials generally provide superior stability and capacity retention compared to exfoliated ones at the same reduction temperature, as demonstrated in both rate capability and long-term cycling tests. The only exception is rGO1000, which exhibits improved rate performance because its increased surface area provides more accessible sodium storage sites. At all other reduction temperatures, exfoliation does not confer performance benefits. For non-exfoliated samples alone, the best performance is observed at an oxygen concentration of roughly 15 wt%. When oxygen content is lower (e.g., rGO600, rGO800, rGO1000), capacity decreases due to insufficient sodium-active sites. On the other hand, when the oxygen level exceeds ~15 wt% (rGO300, rGO200, GO), electrochemical performance also declines, probably because reduced electronic conductivity limits Na^+ transport to deeper storage regions. This observation is consistent with earlier reports linking higher conductivity with greater reduction temperatures [18]. Although rGO400 has somewhat lower conductivity than highly reduced samples, its balance between adequate ionic storage sites and reasonable electronic conductivity results in superior performance.

When compared with prior studies on thermally reduced rGO anodes and with current benchmarks based on hard carbon, the low-surface-area rGO400 exhibits competitive rate capability and ICE, despite requiring milder reduction conditions and retaining a smaller surface area. At present, the highest reported ICE is found in presodiated hard carbon electrodes, produced by immersing dense carbons in a sodium–biphenyl solution [7, 38-40]. While this treatment yields ICE values near 100% in half cells and 95% in full cells, the reversible capacities are lower than those of untreated hard carbon. Moreover, the open-circuit voltage drops significantly from 2.83 V to 0.51 V. Thus, the unusually high ICE should be considered representative of the second cycle, rather than a true first-cycle efficiency, because of the presodiation step.

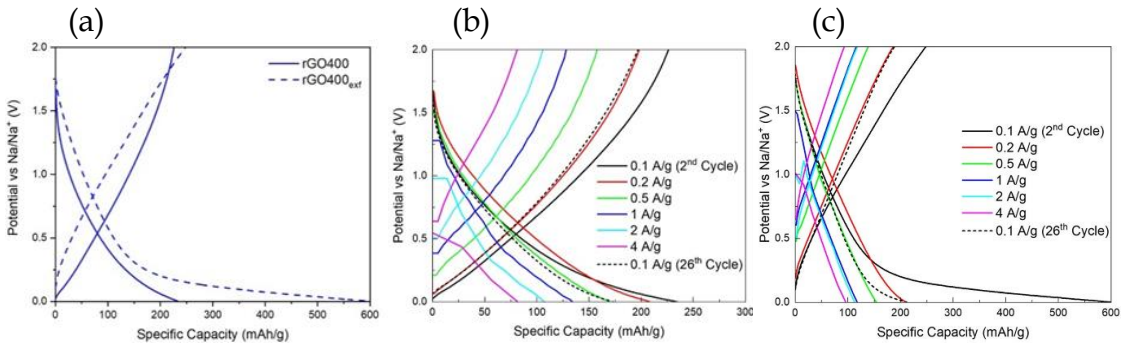

Figure 7. Sodiation/desodiation curves for (a) rGO400 and rGO400exf at 0.1 A g 2., (b) rGO400 at various current densities, and (c) rGO400exf at various current densities. All results are taken with an active mass loading of 0.8 mg cm-2.

CONCLUSIONS AND RECOMMENDATIONS

This work systematically elucidates the influence of specific surface area (SSA) and oxygen content on the electrochemical behavior of reduced graphene oxide (rGO) in sodium-ion batteries. Among all samples, the non-exfoliated rGO reduced at 400 °C exhibited the most favorable performance, which is a novel and significant observation. Its superior behavior arises from an optimized balance between residual oxygen functional groups that generate active storage sites, enlarged interlayer spacing that facilitates Na^+ accommodation, and sufficient electronic conductivity required for stable anode operation.

Contrary to expectations, enhancing SSA through exfoliation did not generally improve electrochemical performance, except at the highest reduction temperature (1000 °C). At this condition, the increased surface area became beneficial only after sufficient storage sites were created, as evidenced by rGO1000. However, exfoliated samples consistently showed lower initial Coulombic efficiency (ICE) than their non-exfoliated counterparts because their large surface area promoted excessive solid–electrolyte interphase (SEI) growth, leading to irreversible Na^+ consumption.

From a processing perspective, exfoliated materials also posed practical drawbacks: their slurries displayed higher viscosity, were more difficult to cast uniformly, and required larger amounts of solvent due to folding and stacking of exfoliated sheets. Non-exfoliated materials, by contrast, enabled fabrication of slurries with greater solid loading, offering advantages in electrode processing. Overall, non-exfoliated rGO consistently outperformed exfoliated samples in terms of ICE, rate capability, cycle stability, and manufacturability, with the sole exception of rGO1000exf, which exceeded the non-exfoliated version in rate performance.

REFERENCES

Cao, Y., et al. (2012). Sodium ion insertion in hollow carbon nanowires for battery applications. Nano Letters, 12(7), 3783–3787. https://doi.org/10.1021/nl3016957

Cheng, D., et al. (2021). Electrochemical storage mechanism of sodium in carbon materials: A study from soft carbon to hard carbon. Carbon, 182, 758–769. https://doi.org/10.1016/j.carbon.2021.06.066

Fan, X., Kong, X., Zhang, P., & Wang, J. (2024). Research progress on hard carbon materials in advanced sodium-ion batteries. Energy Storage Materials, 69, 103386. https://doi.org/10.1016/j.ensm.2024.103386

Fu, H., Xu, Z., Guan, W., Shen, X., Cao, L., & Huang, J. (2018). Adsorption contributions of graphene to sodium ion storage performance. Journal of Physics D: Applied Physics, 51(20), 205501. https://doi.org/10.1088/1361-6463/aabc4b

Guex, L. G., et al. (2017). Experimental review: Chemical reduction of graphene oxide (GO) to reduced graphene oxide (rGO) by aqueous chemistry. Nanoscale, 9(27), 9562–9571. https://doi.org/10.1039/C7NR02943H

Hummers, W. S., & Offeman, R. E. (1958). Preparation of graphitic oxide. Journal of the American Chemical Society, 80(6), 1339. https://doi.org/10.1021/ja01539a017

Hummers, W. S., & Offeman, R. E. (1958). Preparation of graphitic oxide. Journal of the American Chemical Society, 80(6), 1339. https://doi.org/10.1021/ja01539a017

Jiříčková, A., Jankovský, O., Sofer, Z., & Sedmidubský, D. (2022). Synthesis and applications of graphene oxide. Materials, 15(3), 920. https://doi.org/10.3390/ma15030920

Khan, Z. U., & Atif, M. (2025a). Electrochemical investigation of bimetallic oxide-carbon composite electrode: Towards enhanced supercapacitor applications. Next Research, Article 100815.

Khan, Z. U., et al. (2024b). Fabrication of copper-doped lignin-based carbon nanotube composite electrodes for energy storage applications. In 2024 21st International Bhurban Conference on Applied Sciences and Technology (IBCAST). IEEE.

Khan, Z. U., et al. (2025d). Electrolyte effect on electrochemical behaviors of bimetallic metal-organic framework/reduced graphene oxide composite for an energy storage application. Journal of Energy Storage, 134, Article 118189.

Khan, Z. U., et al. (2025e). Fabrication of cobalt-doped lignin base carbon nanotubes composite material for energy storage applications. Journal of the Chemical Society of Pakistan, 47(4).

Khan, Z. U., Jiang, J., & Atif, M. (2025b). Nanostructured bimetallic oxide/graphene nanocomposites for next-generation high-performance energy storage. International Journal of Environmental Research, 19(223).

Khan, Z. U., Jiang, J., & Khan, M. Y. A. (2024a). A comprehensive review on recent advancements in new carbon and metal-organic framework base energy storage materials and devices. Journal of Energy Storage, 100, Article 113464.

Khan, Z. U., Jiang, J., & Ullah, Z. (2024c). A facile synthesis of Co-doped ZnO/rGO nanomaterials for energy storage applications. In 2024 IEEE PES 16th Asia-Pacific Power and Energy Engineering Conference (APPEEC). IEEE.

Khan, Z. U., Jiang, J., & Zeb, S. (2026). Nanostructured zinc-doped nickel/iron metal–organic framework electrode material for an efficient energy storage. Journal of Materials Science: Materials in Electronics, 37(152).

Khan, Z. U., Jiang, J., Ullah, Z., Khan, M. Y. A., & Kusar, A. (2025c). Fabrication of cobalt-doped lignin base carbon nanotubes composite material for energy storage applications. Journal of the Chemical Society of Pakistan, 47.

Lee, W.-J., Jang, H.-R., Kim, M.-J., Kim, H.-M., Oh, J.-M., & Paek, S.-M. (2019). Microwave-irradiated reduced graphene oxide nanosheets for highly reversible and ultrafast sodium storage. Journal of Alloys and Compounds, 778, 382–390. https://doi.org/10.1016/j.jallcom.2018.11.173

Li, F., Wei, Z., Manthiram, A., Feng, Y., Ma, J., & Mai, L. (2019). Sodium-based batteries: From critical materials to battery systems. Journal of Materials Chemistry A, 7(16), 9406–9431. https://doi.org/10.1039/C8TA11999F

Li, J., et al. (2017). Novel iodine-doped reduced graphene oxide anode for sodium ion batteries. RSC Advances, 7(87), 55060–55066. https://doi.org/10.1039/C7RA09349G

Liu, L., Xu, Q., Yin, S., Liu, Z., Li, Y., & Pang, W. (2024). Recent progress on hard carbon-based anode for sodium-ion battery. Journal of Power Sources, 615, 235116. https://doi.org/10.1016/j.jpowsour.2024.235116

Liu, M., et al. (2020). Chemically presodiated hard carbon anodes with enhanced initial coulombic efficiencies for high-energy sodium ion batteries. ACS Applied Materials & Interfaces, 12(15), 17620–17627. https://doi.org/10.1021/acsami.0c02230

Liu, X., et al. (2024). Potato-starch-based hard carbon microspheres: Preparation and application as an anode material for sodium-ion batteries. Solid State Ionics, 406, 116475. https://doi.org/10.1016/j.ssi.2024.116475

Luo, D., et al. (2018). Surface-dominated sodium storage towards high capacity and ultrastable anode material for sodium-ion batteries. Advanced Functional Materials, 28(47). https://doi.org/10.1002/adfm.201805371

Ma, Y., et al. (2024). Hydrothermal synthesis of $(NH_4)_2V_7O_{16}$/reduced graphene oxide composite with enhanced storage performance for aqueous lithium-ion batteries. Energy Technology, 12(7). https://doi.org/10.1002/ente.202301595

Marcano, D. C., et al. (2010). Improved synthesis of graphene oxide. ACS Nano, 4(8), 4806–4814. https://doi.org/10.1021/nn1006368

McAllister, M. J., et al. (2007). Single sheet functionalized graphene by oxidation and thermal expansion of graphite. Chemistry of Materials, 19(18), 4396–4404. https://doi.org/10.1021/cm0630800

Müllner, S., et al. (2023). Impact of functional groups in reduced graphene oxide matrices for high energy anodes in lithium-ion batteries. Journal of The Electrochemical Society, 170(7), 070523. https://doi.org/10.1149/1945-7111/ace70a

Pang, J., Li, J., Guo, J., Jia, M., & Zhang, J. (2023). Tuning the aggregation structure and surface composition of reduced graphene oxide microspheres for high-rate supercapacitors. Diamond and Related Materials, 136, 109920. https://doi.org/10.1016/j.diamond.2023.109920

Qiu, Y., Moore, S., Hurt, R., & Külaots, I. (2017). Influence of external heating rate on the structure and porosity of thermally exfoliated graphite oxide. Carbon, 111, 651–657. https://doi.org/10.1016/j.carbon.2016.10.051

Ramesha, G. K., & Sampath, S. (2009). Electrochemical reduction of oriented graphene oxide films: An in situ Raman spectroelectrochemical study. The Journal of Physical Chemistry C, 113(19), 7985–7989. https://doi.org/10.1021/jp811377n

Schniepp, H. C., et al. (2006). Functionalized single graphene sheets derived from splitting graphite oxide. The Journal of Physical Chemistry B, 110(17), 8535–8539. https://doi.org/10.1021/jp060936f

Stankovich, S., et al. (2007). Synthesis of graphene-based nanosheets via chemical reduction of exfoliated graphite oxide. Carbon, 45(7), 1558–1565. https://doi.org/10.1016/j.carbon.2007.02.034

Usiskin, R., et al. (2021). Fundamentals, status and promise of sodium-based batteries. Nature Reviews Materials, 6(11), 1020–1035. https://doi.org/10.1038/s41578-021-00324-w

Wang, Y.-X., Chou, S.-L., Liu, H.-K., & Dou, S.-X. (2013). Reduced graphene oxide with superior cycling stability and rate capability for sodium storage. Carbon, 57, 202–208. https://doi.org/10.1016/j.carbon.2013.01.064

Wu, C., et al. (2024). Hard carbon for sodium-ion batteries: Progress, strategies and future perspective. Chemical Science, 15(17), 6244–6268. https://doi.org/10.1039/D4SC00734D

Yan, L., Yu, J., & Luo, H. (2017). Ultrafine TiO_2 nanoparticles on reduced graphene oxide as anode materials for lithium ion batteries. Applied Materials Today, 8, 31–34. https://doi.org/10.1016/j.apmt.2017.02.001

Zhao, X., et al. (2023). Impact of surface structure on SEI for carbon materials in alkali ion batteries: A review. Batteries, 9(4), 226. https://doi.org/10.3390/batteries9040226

Zheng, H., et al. (2024). ICE optimization strategies of hard carbon anode for sodium-ion batteries: From the perspective of material synthesis. Materials Futures, 3(3), 032102. https://doi.org/10.1088/2752-5724/ad5d7f

Zhu, Y., Murali, S., Stoller, M. D., Velamakanni, A., Piner, R. D., & Ruoff, R. S. (2010). Microwave assisted exfoliation and reduction of graphite oxide for ultracapacitors. Carbon, 48(7), 2118–2122. https://doi.org/10.1016/j.carbon.2010.02.001